Desalination and Water Treatment
www.deswater.com

doi: 10.5004/dwt.2018.21956

108 (2018) 216–222
March

Bicarbonate-enhanced removal of a typical amino acid using a cobalt(II)-catalyzed Fenton-like reaction in aqueous solution

Cheng Liu[a,b,*], Meiqi Zhao[b], Siyuan He[b], Zhen Cao[b], Wei Chen[b]

[a]*Key Laboratory of Integrated Regulation and Resource Development on Shallow Lakes, Ministry of Education, Hohai University, Nanjing 210098, China, Tel. +86 18913959968; Fax: +86 25 83787618; email: liucheng8791@hhu.edu.cn*
[b]*College of Environment, Hohai University, Nanjing 210098, China, emails: 644503269@qq.com (M. Zhao), 2499737405@qq.com (S. He), 771674813@qq.com (Z. Cao), 107489860@qq.com (W. Chen)*

Received 11 September 2017; Accepted 24 January 2018

ABSTRACT

Dissolved organic nitrogen (DON) has drawn more attention because of its potential to form nitrogenous disinfection by-products. Amino acids are important DON constituents in alkaline eutrophic water. Alkaline water interferes with advanced oxidation processing of target compounds. A new oxidation process using the H_2O_2–HCO_3^- system was used to remove the typical amino acid histidine from water. The rates of DON and histidine removal in the Co^{2+}/H_2O_2–HCO_3^- system within 60 min were 54% and 72%, respectively. The optimum pH for histidine degradation was 8, and the optimal dosages of $NaHCO_3$ and H_2O_2 were 35 and 20 mM, respectively. Co(II) complex with amino acids (Co(II)–Xaa complex), •OH, and HCO_4^- were involved in the degradation, and $•O_2$ formed via HCO_4^- decomposition, as evidenced by the previous study. The reaction products suggest that part of the histidine undergoes oxidation to ammonia nitrogen within 60 min. High-performance liquid chromatography–mass spectrometry results reveal that histidine degradation consists of two separate pathways involving the Co(II)–Xaa complex, •OH, and $•O_2^-$, with the two pathways gradually converting $–NH_2$ into NH_4^+–N. Gas chromatography detection showed that the nitrogenated-disinfection by-products formation rate decreased in the Co^{2+}/H_2O_2–HCO_3^- system.

Keywords: Cobalt; Bicarbonate; Hydrogen peroxide; Dissolved organic nitrogen; Histidine; Drinking water

1. Introduction

Dissolved organic nitrogen (DON) has been the focus of a number of studies on drinking water treatment because of its potential to form nitrogenous disinfection by-products [1–4], which are far more carcinogenic or mutagenic than some of the regulated disinfection by-products (DBPs) [5]. Amino acids are an important component of DON. Amino acids and proteins are important and common organic nitrogen components in water, especially raw water with high algal content. Liu et al. [6] and Takaara et al. [7] showed that there are 185 kinds of protein and 17 free amino acids in water samples derived from *Microcystis aeruginosa* cells. Previous studies have revealed that amino acids have great potential for forming nitrogenated-DBPs (N-DBPs) during chlorination of drinking water [8,9]. Since conventional drinking water treatment processes preferentially remove high-molecular-weight DON, low-molecular-weight amino acids may still be present in the water prior to chlorination disinfection [10]. Therefore, removing amino acids before disinfection aids the control of N-DBP formation. Methods for this purpose thus need to be developed. In this study, histidine was used as the target compound because of its relatively high concentration in raw water and its high potential to form N-DBPs [11].

Advanced oxidation processes are effective at removing many kinds of organic contaminants from water because they generate radicals such as hydroxyl and hydroperoxyl radicals [12]. We have studied the performance of the UV/Cu–TiO_2 system in histidine and DON removal and its

* Corresponding author.

mechanism of removal [13,14]. Although the UV/Cu–TiO_2 system can effectively remove histidine and DON from water, pH seriously affects its removal performance, and higher pH interferes with amino acid removal. Since the pH of most eutrophic water sources is higher than 7.5, bicarbonate (HCO_3^-) is always abundant in such sources. A new advanced oxidation process utilizing bicarbonate that has recently drawn attention uses HCO_3^- as an activator for H_2O_2 in many oxidation reactions to generate many reactive oxygen species such as peroxymonocarbonate (HCO_4^-), hydroxyl radical (•OH) and superoxide radical ($•O_2^-$) [15–17]. Moreover, incorporation of Co^{2+} at micromolar concentrations into the system can markedly increase the degradation rate of organic matter [18–20] such as orange II [21] and methylene blue [22]. However, no study has attempted to use the Co^{2+}/H_2O_2–HCO_3^- system in degrading typical amino acids.

The aim of our research was to investigate the Co^{2+}/H_2O_2–HCO_3^- system's performance in the removal of typical amino acids and the system's removal mechanism. The effects of $NaHCO_3$ dosage, H_2O_2 dosage, pH and the presence of organic compounds on the efficiency of removal were investigated. In order to study the reaction mechanism, electron spin resonance (ESR) experiments and high-performance liquid chromatography–mass spectrometry (HPLC–MS) were conducted to illustrate the main reactive substance and to identify the intermediates. Gas chromatography (GC) experiments were used to determine the formation potential of the N-DBPs dichloroacetonitrile (DCAN) and dichloro acetamide (DCAcAm). The possible reaction pathways and removal mechanism were proposed on the basis of the analysis of experimental data and relevant literature.

2. Materials and methods

2.1. Materials

Reagents were obtained from Sigma-Aldrich Chemical Co., Ltd. (Shanghai, China). All chemicals, which were at least of analytical grade, were used without further purification except when indicated. Methanol (MeOH, HPLC grade) and 5,5-dimethyl-1-pyrrolidine-N-oxide (DMPO) were purchased from Sigma-Aldrich Chemical Co., Ltd. (Shanghai, China) and Sigma-Aldrich (St. Louis, MO, USA), respectively. DCAN was purchased from Sigma-Aldrich (St. Louis, MO, USA), and DCAcAm was obtained from Alfa Aesar (Karlsruhe, Germany). A free chlorine stock solution was prepared from 5% sodium hypochlorite (NaOCl) solution (Sinopharm Chemical Reagent Co., Ltd., Shanghai, China). Relevant properties of the amino acid are shown in Table 1.

Table 1
Relevant properties of histidine

Amino acid	Branched chain	Chemical formula	Molecular weight (g/mol)	Chemical structure
Histidine	Alkaline	$C_6H_9N_3O_2$	155	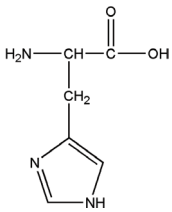

2.2. Analytical methods

NO_3^-, NO_2^-, and NH_4^+ concentrations were measured through a published method [23]. The DON content was determined from the difference between the measured total dissolved nitrogen (TDN) content and the sum of the measured concentrations of dissolved inorganic nitrogen species by using Eq. (1):

$$\text{DON (mg/L)} = \text{TDN} - (NO_3^-\text{–N} + NO_2^-\text{–N} + NH_4^+\text{–N}) \quad (1)$$

Amino acids were analyzed with HPLC using 6-aminoquinolyl-N-hydroxysuccinimidyl (AQC) derivatization [24]. The reaction between AQC, amino acids, and ammonia led to the formation of fluorescent complexes, which were separated on an AccQ-Tag Waters (Shanghai, China) C18 HPLC column (3.924 mm × 150 mm) and then detected at excitation and emission wavelengths of 240 and 395 nm, respectively. The HPLC system consisted of a Waters TM 600 gradient pump, a Merck (Darmstadt, Germany) AS-4000 autosampler, a column heater, and a 474 Waters TM fluorescence detector.

HPLC–MS has been widely used in analytical studies of chemical composition. In the present study, we established a method for the determination of amino acid oxidation products using HPLC–MS. Amino acid oxidation products were identified with ultrahigh-performance liquid chromatography–tandem mass spectrometry (UPLC/MS/MS; Agilent, Waldbronn, Germany). Chromatographic separation was performed at a flow rate of 0.2 mL/min on a Zorbax Eclipse Plus C18 column (2.1 mm × 50 mm, 1.8 μm), which was preceded by a C18 guard column. This column was kept at a temperature of 35°C during the separation. The mobile phase consisted of a 2 mmol/L ammonium acetate solution (eluent A) and acetonitrile (eluent B) filtered through a membrane with a pore size of 0.22 μm. The injection volume was 5 μL. Detection was performed with an Agilent 6460 Series triple quadrupole mass spectrometer equipped with an electrospray ionization source. Qualitative metabolite analysis was conducted by UPLC/MS/MS in full scan mode. Ion-source parameters were as follows: drying temperature of 300°C, drying flow rate of 5 L/min, nebulizer gas pressure of 45 psi, sheath gas temperature of 250°C, sheath gas flow rate of 5 L/min, capillary voltage of 3,500 V, and nozzle voltage of 500 V.

ESR experiments were performed using an EMX-E spectrometer (Bruker, Karlsruhe, Germany) and the spin-trapping agent DMPO. Measurements were carried out under the following conditions: a center field of 3,517 Gs, a sweep width of 100 Gs, a microwave frequency of 20 mW, a modulation amplitude of 1 Gs, and a sweep time of 41.96 s.

GC experiments (Agilent, Waldbronn, Germany) were used to determine the formation potential of the N-DBPs DCAN and DCAcAm. The test method parameters for DCAN were as follows: HP-5 capillary gas chromatographic column (30 m × 0.25 mm × 1 μm), inlet temperature of 250°C, electrical conductivity detector (ECD) temperature of 250°C, high-purity

nitrogen carrier gas (99.99% purity), flow rate of 2 mL/min, tail gas flow rate of 50 mL/min, injection mode for split injection (split ratio 2:1), and sample volume of 1 μL. The test method parameters for DCAcAm were as follows: HP-5 capillary gas chromatographic column (30 m × 0.25 mm × 1 μm), inlet temperature of 235°C; ECD detector temperature of 250°C; high-purity nitrogen carrier gas (99.99% purity), flow rate of 2 mL/min, tail gas flow rate of 50 mL/min, injection mode for splitless injection, and sample volume of 1 μL.

2.3. Experimental procedures

Standard bottle-point methods were used to study the efficiency and mechanism of amino acid catalytic degradation. For the catalytic oxidation experiments, the tests were carried out in 250-mL brown glass bottles held in a constant temperature (25°C ± 1°C) water bath apparatus. In a typical procedure, $NaHCO_3$ was added to 200 mL of amino acid solution (10 mg/L), which was then stirred for 60 min to achieve adsorption–desorption equilibrium. Afterward, the reaction was initiated immediately by addition of H_2O_2 and Co^{2+}. At designated time intervals, a 0.5-mL sample was collected from each bottle and immediately filtered through a 0.22-μm membrane to analyze the concentration of histidine. The sample bottles were pre-filled with 0.2 mL of MeOH solution to quench any residual bicarbonate/hydrogen peroxide-induced oxidation. Residual water samples of each bottle were filtered through cellulose acetate membrane filters with a pore size of 0.45 μm and then transferred to sample vials pre-filled with quencher MeOH, which were used for the determination of DON and N-DBPs. The water sample in each bottle was measured. All experiments were performed in triplicate, and data were reported as mean ± standard deviation.

3. Results and discussion

3.1. Degradation efficiency

Fig. 1 depicts the removal of histidine and DON in the different reaction systems. The Co^{2+}/H_2O_2–HCO_3^- system could catalytically oxidize histidine; the histidine concentration decreased from 10 to 3.2 mg/L within 60 min of the reaction. In contrast, the decrease is higher than the reductions observed in the separate H_2O_2 system (10 to 7.6 mg/L) and in the separate H_2O_2–HCO_3^- system (10–4.5 mg/L). Almost no removal occurred in the $NaHCO_3$ system. The large difference between these different reaction systems shows that addition of Co^{2+} can effectively improve the oxidative ability of the H_2O_2–HCO_3^- system. The increase in histidine oxidation rates may be attributed to active oxygen species such as peroxymonocarbonate (HCO_4^-), hydroxyl radical (•OH), and superoxide radical (•O_2^-) [16]. Co(II) can react with the amino acid and thus form a Co(II)–Xaa complex, which is then oxidized by H_2O_2 to •OH and OH^- [20]. Histidine was oxidized by •OH. Results for DON removal are similar to those for histidine removal. Under the same reaction conditions, the rate of DON removal was lower than that of histidine removal (54% vs. 68%; Fig. 1). This difference may be explained by the incomplete mineralization of amino acids and their consequent incomplete transformation to other organic nitrogen matter, which can be detected as DON. The rate of DON removal indicates that part of the DON underwent direct oxidation to inorganic ions.

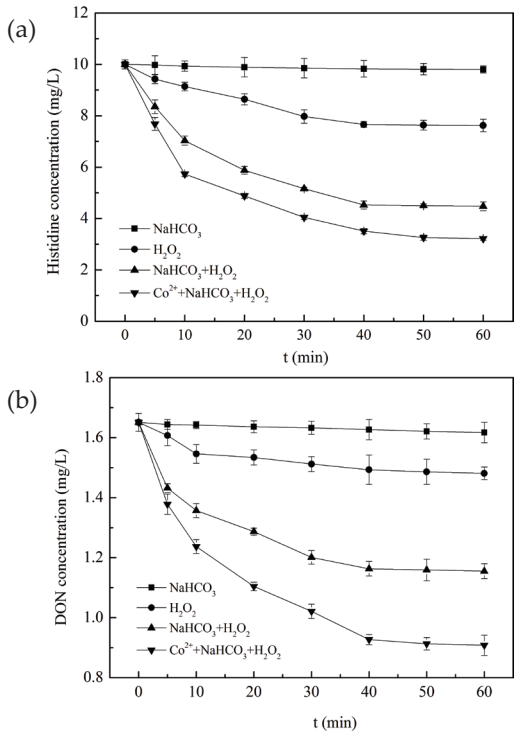

Fig. 1. Efficiency of the different systems in the degradation of (a) histidine and (b) DON (0.1 μM Co^{2+}; 25 mM $NaHCO_3$; 20 mM H_2O_2; pH = 8).

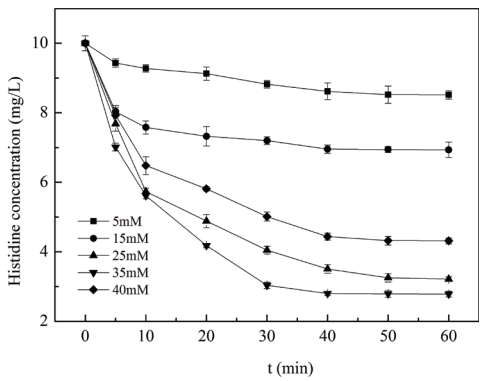

Fig. 2. Effect of $NaHCO_3$ dosage on the degradation efficiency (0.1 μM Co^{2+}; 20 mM H_2O_2; pH = 8).

3.2. Effect of various factors on the catalytic degradation

3.2.1. Effect of $NaHCO_3$ dosage

The rate of histidine removal initially increased and then decreased with the increase in $NaHCO_3$ dosage (Fig. 2). Similar results were obtained in Bokare and Choi's study [20]. When the $NaHCO_3$ dosage was 35 mM, the rate of histidine removal was the highest (72% of histidine after 1 h). However, $NaHCO_3$ dosages that were too high or too low impeded the reaction. When the $NaHCO_3$ dosage was too low (<35 mM), less HCO_3^- participated in the reaction; consequently,

Co^{2+}-catalyzed production of •OH from H_2O_2 was more difficult. When the $NaHCO_3$ dosage was too high (>35 mM), excess HCO_3^- led to a quenching effect. The optimal $NaHCO_3$ dosage was found to be 35 mM.

3.2.2. Effect of H_2O_2 dosage

The effect of H_2O_2 dosage on amino acid degradation is depicted in Fig. 3. With the increase in H_2O_2 concentration, the rate of histidine removal generally increased and then decreased. Fig. 3 shows that when the H_2O_2 concentration increased from 5 to 25 mmol/L, the histidine concentration decreased from 10 to 2.78 mg/L (5–20 mM H_2O_2) and then increased to 3.02 mg/L (25 mM H_2O_2). This trend is due to the sufficient number of active sites on the catalyst when the H_2O_2 concentration is low; an increase in H_2O_2 concentration in the reaction system can lead to production of more •OH, thereby increasing the rate of histidine removal. With further increase in the H_2O_2 concentration, however, an equivalent number of active sites on the catalyst become saturated, thus increasing the amount of H_2O_2 that is not involved in the reaction for •OH production. Similar inhibition has been reported in the literature [20]. Therefore, the optimal H_2O_2 dosage and $NaHCO_3/H_2O_2$ molar ratio are 20 mmol/L and 7:4, respectively (Figs. 2 and 3).

3.2.3. Effect of pH

As is well known, pH is an important factor that affects the Fenton reaction; it is thus necessary to determine the effect of pH on the Co^{2+}/H_2O_2–HCO_3^- system. The effect of pH on amino acid degradation is presented in Fig. 4. The figure shows that the rate of histidine removal increases first and then decreases with the increase in pH, reaching 68% at pH 8. Under acidic conditions such as those at pH 3, a higher removal rate can be obtained with the traditional Fenton reaction. However, only a small amount of HCO_3^- that forms complexes plays an important role in the Co^{2+}/H_2O_2–HCO_3^- system. Too high or too low pH can result in the decomposition of HCO_3^- into CO_3^{2-} or CO_2 and further lead to a decrease in the amount of •OH [20]. According to a previous study [25], the optimum pH for a cobalt-loaded catalyst–HCO_3^-–H_2O_2 system is 8.2, which is similar to our study. Thus, the optimum pH of the Co^{2+}/H_2O_2–HCO_3^- system is 8.0.

3.2.4. Effect of organic compounds

The foregoing experiments were carried out in the presence of amino acids in water. However, the actual compositions of water bodies are highly complex, as they contain various organic compounds. To explore the effect of organic substances in water bodies on the catalytic degradation of amino acids, we added a common organic substance to water samples. Because of the detection index of histidine, the selected organic matter must not contain N. Therefore, 2-propanol was used as the typical organic matter. The degradation rate of histidine decreased with the increase in 2-propanol concentration (Fig. 5). When the 2-propanol dosage was lower, the degradation rate of histidine decreased;

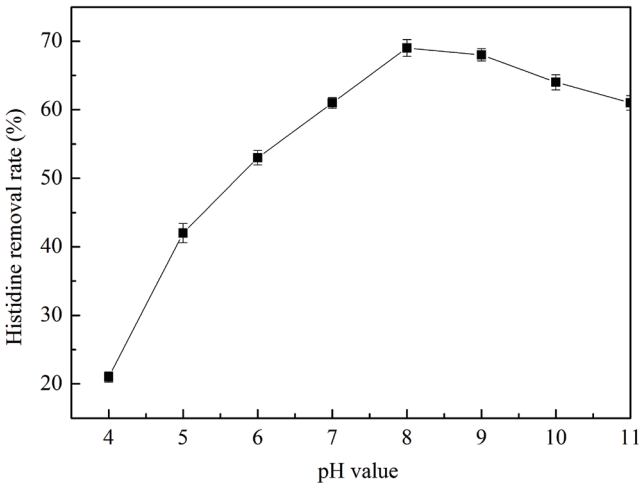

Fig. 4. Effect of pH on the degradation efficiency (0.1 μM Co^{2+}; 35 mM $NaHCO_3$; 20 mM H_2O_2).

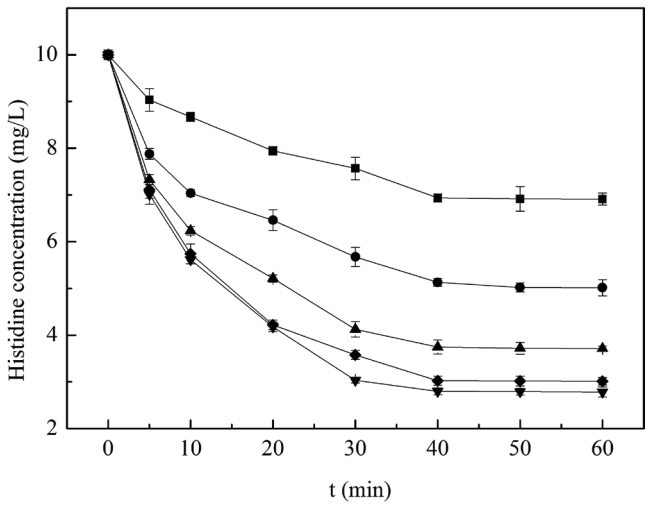

Fig. 3. Effect of H_2O_2 dosage on the degradation efficiency (0.1 μM Co^{2+}; 35 mM $NaHCO_3$; pH = 8).

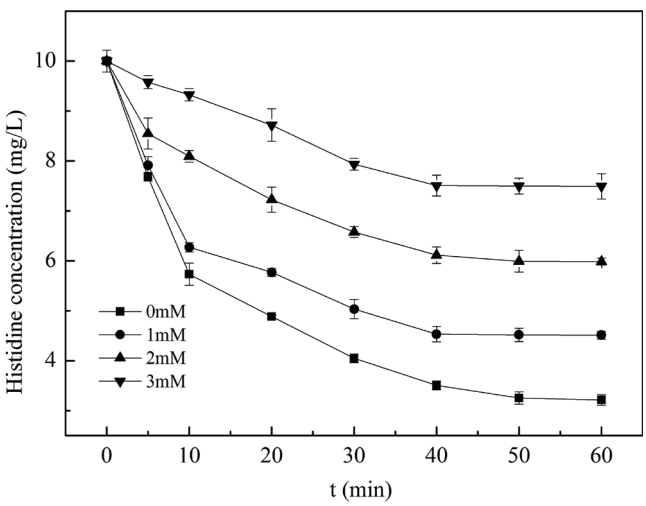

Fig. 5. Effect of 2-propanol concentration on the degradation efficiency (0.1 μM Co^{2+}; 35 mM $NaHCO_3$; 20 mM H_2O_2; pH = 8).

with the increase in 2-propanol concentration, the inhibition of histidine degradation was more obvious. These results imply that histidine degradation mainly involves the generation and participation of •OH radicals in the $Co^{2+}/H_2O_2–HCO_3^-$ system. Similar results were obtained by Luo et al. [26].

3.3. Proposed mechanisms

3.3.1. Behavior of radicals during oxidation

The ESR spectra after 2 min of reaction are shown in Fig. 6. In the spectra of the $H_2O_2–HCO_3^-$ and $Co^{2+}/H_2O_2–HCO_3^-$ systems, characteristic and typical ESR signals of the DMPO–OH adducts at an intensity ratio of 1:2:2:1 are evident as four strong peaks [27] and are lower than those for the peaks of the $Co^{2+}/H_2O_2–HCO_3^-$ system. No ESR signal is present in the spectrum of the separate H_2O_2 system, indicating that HCO_3^- and the $Co^{2+}–HCO_3^-$ system can activate H_2O_2 and thus produce •OH. We detected •OH, which has the hyperfine splitting constants a_N = 14.9 G, a_H = 14.9 G. According to a previous study [16], the active oxygen reactive intermediates may include •OH and $•O_2^-$, with part of the $•O_2^-$ generated by HCO_4^- decomposition. Both radicals facilitate the reaction of histidine. Therefore, results of the ESR experiments and those of the aforementioned study confirm that •OH and $•O_2^-$ can form in the $Co^{2+}/H_2O_2–HCO_3^-$ system, in which •OH plays an important role.

3.3.2. Degradation pathway

The concentrations of TDN, as well as those of nitrogen from NH_4^+, NO_3^-, and NO_2^-, were determined at different reaction times (results are shown in Fig. 7) to confirm the extent of DON oxidation in water. The main forms of nitrogen showed different variation tendencies (Fig. 7). The DON and TDN concentrations decreased, whereas the NH_4^+ concentration increased. No obvious change in the NO_3^- and NO_2^- nitrogen concentrations was detected during the entire oxidation process. According to the concentration variations of TDN, DON, and NH_4^+ (2.65 mg/L vs. 2.10 mg/L, 1.65 mg/L vs. 0.90 mg/L, and 0.038 mg/L vs. 0.44 mg/L), the increase in NH_4^+ nitrogen concentration is caused by histidine oxidation, and NH_4^+ is not converted to nitrogen gas. These results are contrary to those in our former study [12], in which histidine was completely degraded to NH_4^+ and NO_3^-, with NO_3^- finally being reduced to N_2. In this study, these species were removed from water by a UV/Cu–TiO_2 system via a coupling reaction involving photocatalytic oxidation. However, the $Co^{2+}/H_2O_2–HCO_3^-$ system uses homogeneous catalytic oxidation; thus, there is no interaction between NH_4^+ and NO_3^- in its reaction.

HPLC–MS was used to identify the intermediates and final products of amino acid oxidation. According to previous studies [28,29], the amino and carboxyl groups can be simultaneously removed, with carboxylic acid consequently generated in the presence of the catalyst. However, the recovery rate of carboxylic acid was low. Thus, the *m*/*z* ratios of the molecules are shown in Fig. 8.

After catalytic treatment, water samples with the amino acid were analyzed by HPLC–MS (spectra are shown in Fig. 8). The main mass-to-charge (*m*/*z*) ratios in the mass spectrum of the histidine-containing water sample after catalytic treatment are 216.8, 158.7, 139.9, and 114.9 (Fig. 8). The molecular formulas of these substances could be tentatively identified on the basis of the *m*/*z* ratios and the amino acid structure (Table 2).

The aforementioned figures describe oxidative decarboxylation during deamination of histidine.

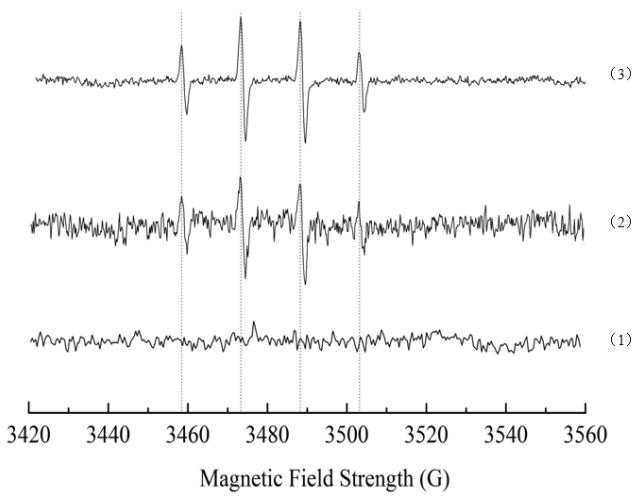

Fig. 6. ESR spectra obtained for the (1) H_2O_2, (2) $H_2O_2–HCO_3^-$, and (3) $Co^{2+}/H_2O_2–HCO_3^-$ systems (0.1 μM Co^{2+}; 35 mM $NaHCO_3$; 20 mM H_2O_2; [DMPO] = 0.1 M).

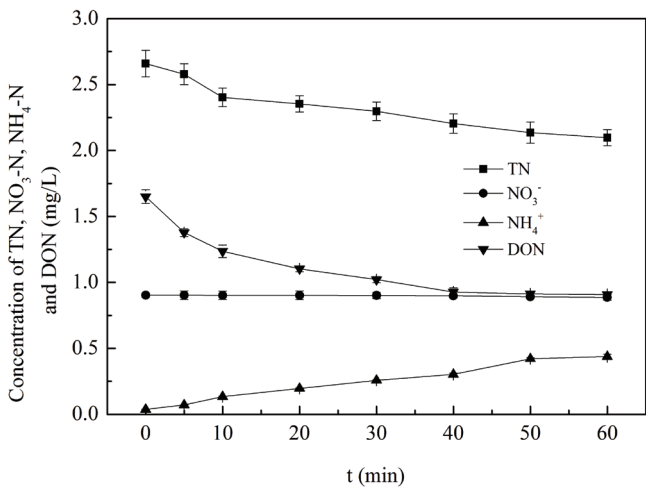

Fig. 7. Changes in TDN, NO_3^-, NH_4^+ concentrations during DON degradation in the $Co^{2+}/H_2O_2–HCO_3^-$ system (0.1 μM Co^{2+}; 35 mM $NaHCO_3$; 20 mM H_2O_2; pH = 8).

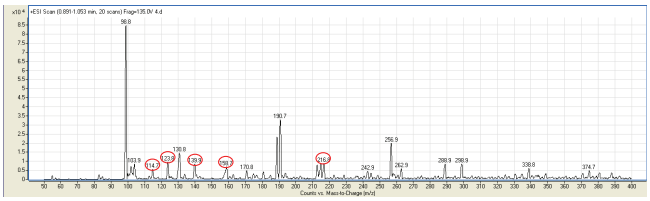

Fig. 8. Mass spectrum of the histidine-containing water sample after the catalytic treatment.

Table 2
Results of the identification of amino acid oxidation products

Amino acid	Monitoring ion	*m/z*	Molecular formula
Histidine	$[M + Na]^+$	158.7	$C_6H_9N_3O_2$
	$[M + H]^+$	139.9	$C_6H_9N_3O$
	$[M + H]^+$	123.8	$C_5H_6N_2O_2$
	$[M + H]^+$	114.7	$C_5H_6N_2O$
	$[M + H]^+$	216.8	Co(II)–Xaa complex

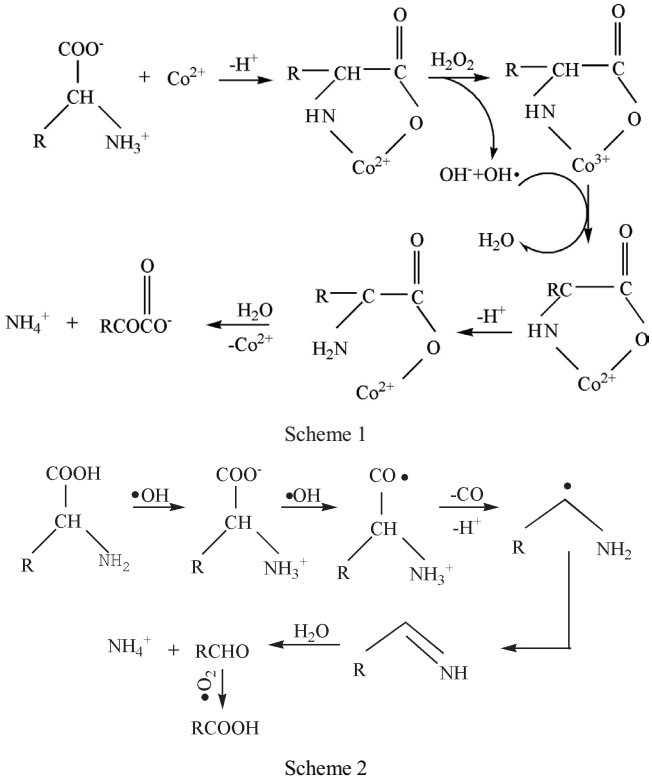

Fig. 9. Degradation of histidine in the Co^{2+}/H_2O_2–HCO_3^- system (0.1 μM Co^{2+}; 35 mM $NaHCO_3$; 20 mM H_2O_2; pH = 8).

As shown in Fig. 9, histidine undergoes degradation via two processes under the action of the Co^{2+}/H_2O_2-HCO_3^- system within 60 min. As shown in scheme 1, Co^{2+} reacts with the amino acid, forming a Co(II)–Xaa complex and liberating a proton. H_2O_2 then oxidizes Co(II) in the complex to form OH•, OH^-, and the Co(III)–Xaa complex [30]. Because OH• formed in close proximity to the amino acid moiety of the complex, it preferentially abstracts a hydrogen atom from the α-carbon of the amino acid to regenerate Co(II) and form the imino acid derivative, which, upon spontaneous hydrolysis, yields the α-keto acid and NH_4^+. Scheme 2 is different from scheme 1 in that the anion undergoes oxidation to carboxyl radical by hydroxyl radical (•OH). Furthermore, α-amino free radical can convert to α-amino carbonium ion to form the protonated imine. Finally, aldehyde can form by hydrolysis. According to previous studies [18], an active $•O_2^-$ intermediate is generated by HCO_4^- decomposition; hence, the aldehyde may be oxidized to carboxylic acid by superoxide radical ($•O_2^-$) [18].

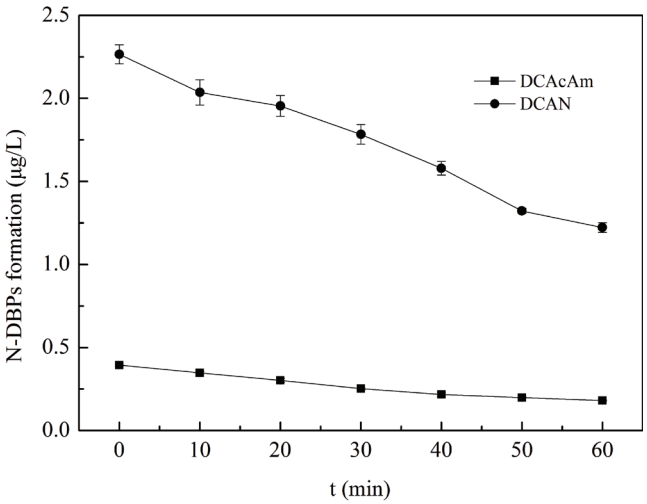

Fig. 10. Formation of N-DBPs during chlorination of histidine at different reaction times in the Co^{2+}/H_2O_2–HCO_3^- system (0.1 μM Co^{2+}; 35 mM $NaHCO_3$; 20 mM H_2O_2; pH = 8).

3.3.3. N-DBP formation

Fig. 10 shows the formation of N-DBPs during chlorination of histidine at different reaction times in the Co^{2+}/H_2O_2–HCO_3^- system. We found that the concentrations of the N-DBPs DCAN and DCAcAm decreased with the increase in reaction time within 60 min. The removal rates of DCAN and DCAcAm were about 51% and 45%, respectively. We can see that the precursor concentrations of DCAN and DCAcAm decreased gradually with the reaction time, and the formation reaction reached completion. Because DCAN had a strong ability to hydrolyze, the concentration of generated DCAN decreased during hydrolysis. This indicates that the rate of N-DBP formation decreased in the Co^{2+}/H_2O_2–HCO_3^- system (Fig. 9).

4. Conclusions

This study is the first that uses bicarbonate-enhanced removal of a typical amino acid through a cobalt(II)-catalyzed hydrogen peroxide reaction during N-DBP degradation. Our results suggest that the Co^{2+}/H_2O_2–HCO_3^- system is effective in the degradation of DON. Under all of the experimental conditions applied, the rate of DON removal within 60 min in the Co^{2+}/H_2O_2–HCO_3^- system is 54%. The optimum pH for histidine degradation is 8. Optimal dosages of $NaHCO_3$ and H_2O_2 are 35 and 20 mM, respectively. The removal rate of amino acid decreases with the increase in 2-propanol concentration. ESR results show that •OH produced by the Co^{2+}/H_2O_2–HCO_3^- system plays an important role. Therefore, DON degradation is a result of oxidation by •OH. Furthermore, the amino acid undergoes degradation within 60 min via two processes in the Co^{2+}/H_2O_2–HCO_3^- system, in which the amino acid is oxidized to α-keto acid, aldehyde, and carboxylic acid. The concentrations of the N-DBPs DCAN and DCAcAm decreased in the Co^{2+}/H_2O_2–HCO_3^- system.

Acknowledgments

This work was supported by the National Natural Science Foundation of China (51378174 and 51438006), and the project funded by the Priority Academic Program Development of Jiangsu Higher Education Institutions.

References

[1] S.D. Richardson, M.J. Plewa, E.D. Wagner, R. Schoeny, D.M. Demarini, Occurrence, genotoxicity, and carcinogenicity of regulated and emerging disinfection by-products in drinking water: a review and roadmap for research, Mutat. Res., 636 (2007) 178–242.

[2] J.J. Rook, Formation of haloforms during chlorination of natural water, Water Treat. Exam., 23 (1974) 234–243.

[3] T.A. Bellar, R.C. Kroner, The occurrence of organohalides in chlorinated drinking water, J. Am. Water Works Assoc., 66 (1974) 703–706.

[4] F. Darwin, D.F.M. Pertz, Determination of the aqueous chlorination products of humic substances by gas chromatography with microwave plasma emission detection, Anal. Chem., 52 (1980) 257–284.

[5] M.J. Plewa, E.D. Wagner, P. Jazwierska, S.D.R. And, P.H. Chen, A.B. Mckague, Halonitromethane drinking water disinfection byproducts: chemical characterization and mammalian cell cytotoxicity and genotoxicity, Environ. Sci. Technol., 38 (2004) 62–68.

[6] C. Liu, J. Wang, W. Chen, H. Zhu, H. Bi, Characterization of DON in IOM derived from *M. aeruginosa* and its removal by sunlight/immobilized TiO_2 system, RSC Adv., 5 (2015) 41203–41209.

[7] T. Takaara, D. Sano, Y. Masago, T. Omura, Surface-retained organic matter of *Microcystis aeruginosa* inhibiting coagulation with polyaluminum chloride in drinking water treatment, Water Res., 44 (2010) 3781–3786.

[8] I.K. Konstantinou, T.A. Albanis, TiO_2-assisted photocatalytic degradation of azo dyes in aqueous solution: kinetic and mechanistic investigations: a review, Appl. Catal., B, 49 (2004) 1–14.

[9] C.S. Uyguner-Demirel, M. Bekbolet, Significance of analytical parameters for the understanding of natural organic matter in relation to photocatalytic oxidation, Chemosphere, 84 (2001) 1009–1031.

[10] M. Tomaszewska, S. Mozia, Removal of organic matter from water by PAC/UF system, Water Res., 36 (2002) 4137–4143.

[11] X. Yang, Q. Shen, W. Guo, J. Peng, Y. Liang, Precursors and nitrogen origins of trichloronitromethane and dichloroacetonitrile during chlorination/chloramination, Chemosphere, 88 (2012) 25–32.

[12] N. Daneshvar, V. Vatanpour, S. Aber, M.H. Rasoulifard, Electro-Fenton treatment of dye solution containing Orange II: influence of operational parameters, J. Electroanal. Chem., 615 (2008) 165–174.

[13] C. Liu, J. Wang, W. Chen, Z. Sun, Z. Cao, Performance and mechanism of UV/immobilized Cu-TiO_2 system to degradation histidine, J. Nanomater., 2016 (2016) 1–9.

[14] C. Liu, J. Wang, W. Chen, C. Dong, C. Li, The removal of DON derived from algae cells by Cu-doped TiO_2 under sunlight irradiation, Chem. Eng. J., 280 (2015) 588–596.

[15] B. Balagam, D.E. Richardson, The mechanism of carbon dioxide catalysis in the hydrogen peroxide N-oxidation of amines, Inorg. Chem., 47 (2008) 1173.

[16] J.M. Lin, M. Liu, Singlet oxygen generated from the decomposition of peroxymonocarbonate and its observation with chemiluminescence method, Spectrochim. Acta A, 72 (2009) 126–132.

[17] A. Xu, X. Li, H. Xiong, G. Yin, Efficient degradation of organic pollutants in aqueous solution with bicarbonate-activated hydrogen peroxide, Chemosphere, 82 (2011) 1190–1195.

[18] A. Jawad, Z. Chen, G. Yin, Bicarbonate activation of hydrogen peroxide: a new emerging technology for wastewater treatment, Chin. J. Catal., 37 (2016) 810–825.

[19] J. Peng, H. Shi, J. Li, L. Wang, Z. Wang, S. Gao, Bicarbonate enhanced removal of triclosan by copper(II) catalyzed Fenton-like reaction in aqueous solution, Chem. Eng. J., 306 (2016) 484–491.

[20] A.D. Bokare, W. Choi, Bicarbonate-induced activation of H_2O_2 for metal-free oxidative desulfurization, J. Hazard. Mater., 304 (2016) 313–319.

[21] X. Guo, H. Li, S. Zhao, Fast degradation of Acid Orange II by bicarbonate-activated hydrogen peroxide with a magnetic S-modified $CoFe_2O_4$, catalyst, J. Taiwan Inst. Chem. Eng., 55 (2015) 90–100.

[22] A. Xu, X. Li, S. Ye, G. Yin, Q. Zeng, Catalyzed oxidative degradation of methylene blue by in situ generated cobalt (II)-bicarbonate complexes with hydrogen peroxide, Appl. Catal., B, 102 (2011) 37–43.

[23] State Environmental Protection Administration of China, Monitoring and Analysis Methods of Water and Wastewater, 4th ed., Environmental Science Press, Beijing, China, 2002.

[24] J. Díaz, J.L. Lliberia, L. Comellas, F. Broto-Puig, Amino acid and amino sugar determination by derivatization with 6-aminoquinolyl-N-hydroxysuccinimidyl carbamate followed by high-performance liquid chromatography and fluorescence detection, J. Chromatogr. A, 719 (1996) 171–179.

[25] Z. Li, W. Song, Z. Chen, G. Yin, Degradation of organic pollutants in wastewater by bicarbonate-activated hydrogen peroxide with a supported cobalt catalyst, Environ. Sci. Technol., 47 (2013) 3833.

[26] M. Luo, L. Lv, G. Deng, W. Yao, R. Yang, X. Li, A. Xu, The mechanism of bound hydroxyl radical formation and degradation pathway of Acid Orange II in Fenton-like Co^{2+}-HCO_3^-, system, Appl. Catal., A, 469 (2014) 198–205.

[27] X. Li, Z. Xiong, X. Ruan, D. Xia, Q. Zeng, A. Xu, Kinetics and mechanism of organic pollutants degradation with cobalt–bicarbonate–hydrogen peroxide system: investigation of the role of substrates, Appl. Catal., A, 411 (2011) 24–30.

[28] A.O. Allen, C.J. Hochanadel, J.A. Ghormley, T.W. Davis, Decomposition of water and aqueous solutions under mixed fast neutron and γ-radiation, J. Phys. Chem., 56 (1951) 575–586.

[29] W. Chu, J. Hu, T. Bond, N. Gao, B. Xu, D. Yin, Water temperature significantly impacts the formation of iodinated haloacetamides during persulfate oxidation, Water Res., 98 (2016) 47–55.

[30] B.S. Berlett, P.B. Chock, M.B. Yim, E.R. Stadtman, Manganese(II) catalyzes the bicarbonate-dependent oxidation of amino acids by hydrogen peroxide and the amino acid-facilitated dismutation of hydrogen peroxide, Proc. Natl. Acad. Sci. USA, 87 (1990) 389–393.